Available online at www.sciencedirect.com

ScienceDirect

Russian Geology and Geophysics 58 (2017) 844–854

RUSSIAN GEOLOGY AND GEOPHYSICS

www.elsevier.com/locate/rgg

Determination of corner frequencies of source spectra for subduction earthquakes in Avacha Gulf (*Kamchatka*)

A.A. Skorkina [a,b,*], A.A. Gusev [a,c]

[a] *Kamchatka Branch of the Geophysical Survey, Russian Academy of Sciences, bul'v. B. Piipa 9, Petropavlovsk-Kamchatskii, 683006, Russia*

[b] *The Schmidt Institute of Physics of the Earth, Russian Academy of Sciences, ul. B. Gruzinskaya 10/1, Moscow, 123242, Russia*

[c] *Institute of Volcanology and Seismology, Far Eastern Division, Russian Academy of Sciences, bul'v. B. Piipa 9, Petropavlovsk-Kamchatskii, 683006, Russia*

Received 3 June 2016; accepted 20 October 2016

Abstract

The source spectra of $M = 4.0$–6.5 subduction earthquakes of 2011–2014 in Kamchatka are studied. The dataset comprises 1272 source spectra recovered from S waves of 372 earthquakes recorded by six digital rock-ground stations. The structure of the spectra is examined on the basis of a spectral model with three corner frequencies f_{c1}, f_{c2}, and f_{c3}. It was assumed that the spectra behave as f^{-2} between f_{c2} and f_{c3}, where f_{c3} denotes "source-controlled f_{max}" after Aki and Gusev. To determine the corner frequencies, we extracted the source spectra from S-wave spectra using a previously developed attenuation model for the study area. The spectra were first reduced to the reference hard-rock station, employing a specially determined set of spectral amplifications of stations. We approximated the recovered source spectrum by a piecewise power-law function, estimated f_{c1}, f_{c2}, and f_{c3}, and examined their dependence on the seismic moment M_0 (i.e., scaling). The dependence $f_{c1}(M_0)$ does not contradict the hypothesis of source similarity when one expects $f_{c1} \propto M_0^{-1/3}$. For f_{c2} and f_{c3}, the scaling is close to $f_{c2} \propto M_0^{-0.23}$ and $f_{c3} \propto M_0^{-0.13}$, respectively, indicating a clear violation of the similarity, especially prominent for f_{c3}. Systematic identification of the frequency f_{c3}, its determination, and analysis of its scaling are the main results of the study, important for understanding the physics of earthquake source processes. The use of f_{c3} as a source parameter in strong ground motion simulations will eliminate biases in estimating attenuation parameters, in particular, the spectral decay parameter "kappa".

Keywords: earthquake; source spectra; scaling law; third corner frequency; f_{max}; source-controlled f_{max}; kappa

Introduction

The study of earthquake source spectra is of interest to earthquake source physics and is important for the solution of engineering seismology problems. In theory, a source displacement spectrum (SDS) is described by the level of the flat part of the spectrum and position of its crossover points or corner frequencies. The standard model of the source displacement spectrum is the omega-square (ω^{-2}) model (Aki, 1967; Brune, 1970), which includes a flat ($\propto f^0$) segment at low frequencies (LF) and a falloff at high frequencies (HF). These two segments are separated by a crossover at the corner frequency f_c. As early as in (Brune, 1970), it was noted that this corner can be split into two; the corresponding corner frequencies will be denoted by f_{c1} and f_{c2}. The frequent occurrence of a crossover at f_{c2} is known (Gusev, 1983, 2012; Papageorgiou and Aki, 1983; and others), but the properties of f_{c2} are not well understood.

Source acceleration spectra (SAS), which increase as f^2 at LF and have two crossovers at f_{c1} and f_{c2} and a plateau ($\propto f$) at $f > f_{c2}$ are useful for many purposes. In acceleration spectra, this plateau is always followed on the right by an upper (HF) cutoff of the spectrum. In the ω^{-2} model, this cutoff is usually attributed to an increase in ray path loss with increasing frequency. If the loss is known, it can be taken into account, so that the source spectrum recovered from observations should be flat. In practice, after the described correction of HF, the cutoff typically persists; in (Hanks, 1982), the cutoff frequency of such a residual cutoff is denoted as f_{max}. In (Gusev, 1983; Papageorgiou and Aki, 1983), the formation of this cutoff is attributed to the source (see the discussion in (Gusev, 2012). Soon, however, it was shown (Anderson and Hough, 1984) that its probable cause is the intrinsic loss in the near-surface layers. This loss is characterized by the

* Corresponding author.
E-mail address: anna@emsd.ru (A.A. Skorkina)

1068-7971/$ - see front matter
http://dx.doi.org/10.1016/j.rgg.2017.06.007

quantity κ_0 ($\kappa_0 = \int_l dt/Q$, where l is the short segment of the ray directly beneath the station). However, it has been systematically found that f_{max} can be detected in acceleration spectra corrected for both types of loss: along most of the ray path and directly beneath the station. These facts indicate that f_{max} is partly of source origin. The contribution of the source to the generation of f_{max} is now generally recognized in principle (Purvance and Anderson, 2003), but the issue has been studied insufficiently.

The complex nature of the phenomenon has led to the emergence of awkward terms: 1) site (station)-controlled f_{max} and 2) source-controlled f_{max}; hereinafter, they will be denoted as (1) f_κ and (2) f_{c3}, i.e., the third corner frequency. The latter parameter is an important subject of this study. There are still no approaches that would allow a reliable and systematic separation of the contributions of f_κ and f_{c3} to the observed f_{max} effect. It is believed that by determining and compensating for the wave propagation loss, it is possible to establish the reality of the upper cutoff of SAS and, in case of success, obtain numerical estimates for f_{c3}. For the Avacha Gulf region in East Kamchatka, the loss parameters of the medium ($Q(f)$ and κ_0) were reliably estimated in (Gusev and Guseva, 2016a). These estimates of the loss can be used to correct station spectra in this region.

Mass estimates of f_{c2} and f_{c3} for Kamchatka were first obtained from the data of the single PET station for 1993–2005 (Gusev and Guseva, 2014) using a preliminary loss model. However, due to the limited reliability of these results and the overall low knowledge of the parameters f_{c2} and f_{c3}, this work should be performed at a new level. It employs refined estimates of the intrinsic loss in the medium and a network of stations instead of a single station. In 2008–2010, a network of stations was organized for the Avacha Gulf region, providing an opportunity to carry out such study, to be described below.

Initial data set

By 2011, a digital seismic network which uses CMG5T and CMG5TD accelerometers was deployed in Kamchatka (Chebrov et al., 2013). To study earthquake source spectra in the region, we processed records of such instruments located on rock or hard ground at the Dal'niy (DAL), Khodutka (KDT), Karymshina (KRM), Petropavlovsk (PET), Russkaya (RUS), and Shipunskii (SPN) stations in the Avacha Gulf region in 2011–2014 (Fig. 1*a*). The range of hypocentral distances r is 45–250 km, mainly over 75 km (Fig. 1*b*), the depths are up of 170 km, mainly up to 50 km, and the range of magnitudes M_L is 4.0–6.8. Records of 372 subduction earthquakes were processed. Records with high noise levels or multiple events were excluded.

The absence of records at distances less than 50–70 km from the stations (Fig. 1*b*) is a specific property of subduction earthquake records obtained in Kamchatka: their sources are beneath the ocean floor, and the stations are on the coast. Processing of such data does not always provide full information about the source and medium, and this has to be accepted.

Principles of conversion of observed spectra to the source

To validate the employed data analysis technique, it is necessary to consider the earthquake source, the source spectrum, and its relationship to the station record (signal).

The case of a homogeneous lossless medium (ideal case). In this paper, the internal structure of earthquake sources is not considered. An earthquake source is described using an equivalent point source—a double couple whose scalar seismic moment increases according to a law $M_0(t)$; the rate of its increase is $\dot{M}_0(t)$. The amplitude spectrum of $\dot{M}_0(t)$ will be denoted as $\dot{M}_0(f)$; it is called the source spectrum. The seismic moment as a numerical parameter of the source is $M_0 = M_0(t)\big|_{t=\infty} = \dot{M}_0(f)\big|_{f=0}$. Up to a factor, the functions $\dot{M}_0(t)$ and $\dot{M}_0(f)$ coincide, respectively, with the time history $D(t)$ and spectrum $D(f)$ of the body-wave displacement signal in the ideal case of a homogeneous unbounded elastic lossless medium. In this case,

$$D(t) = A_1 \dot{M}(t - r/c_S); \quad A_1 = \frac{R_S}{4\pi\rho c_S^3 r}, \tag{1}$$

where R_S is the radiation pattern for the S wave displacement (below, we use the value $R_S{}^2 = 0.4$ averaged over the source sphere) and ρ and c_S are the density and velocity of S waves. It is also useful to introduce the function $\dot{M}_0(f)$ related to the spectrum $V(f)$ of the velocity signal $\dot{V}(t)$, and the source acceleration spectrum $\ddot{M}_0(f) = (2\pi f)^2 \dot{M}_0(f)$ related to the spectrum $A(f)$ of the acceleration signal $A(t)$. In studies of real sources, the calculated signal spectra have to be smoothed (averaged over a limited frequency band), which is justified by the absence of distinct systematic peaks and troughs in the observed spectra. To recover source spectra from real records, the recorded spectra had to be reduced to the ideal conditions described above.

Approximate characteristics of real cases. In practice, in addition to (1), there are several effects more, which will be described by using additional factors on the right side of (1). These include:

1.1. The free surface effect, factor $C_{11} \approx 2.0$.

1.2. Projection of the S wave displacement vector onto the direction of the receiver component C_{12}. We worked with spectra of the horizontal components and set $C_{12}^2 = 0.5$.

1.3. Ray curvature. Its effect can be written as the factor $C_{13} = G(r)/r$. Under our conditions, this factor is difficult to estimate reliably as the form of records is hardly consistent with the principles of geometric seismics. We will set $C_{13} = 1$.

2.1. The influence of the ratio of the impedances (acoustic stiffnesses) of the medium near the source (0) and receiver (1), $C_{21}(f) = (c_S^{(0)}\rho^{(0)}/c_S^{(1)}\rho^{(1)})^{0.5}$. This factor depends on

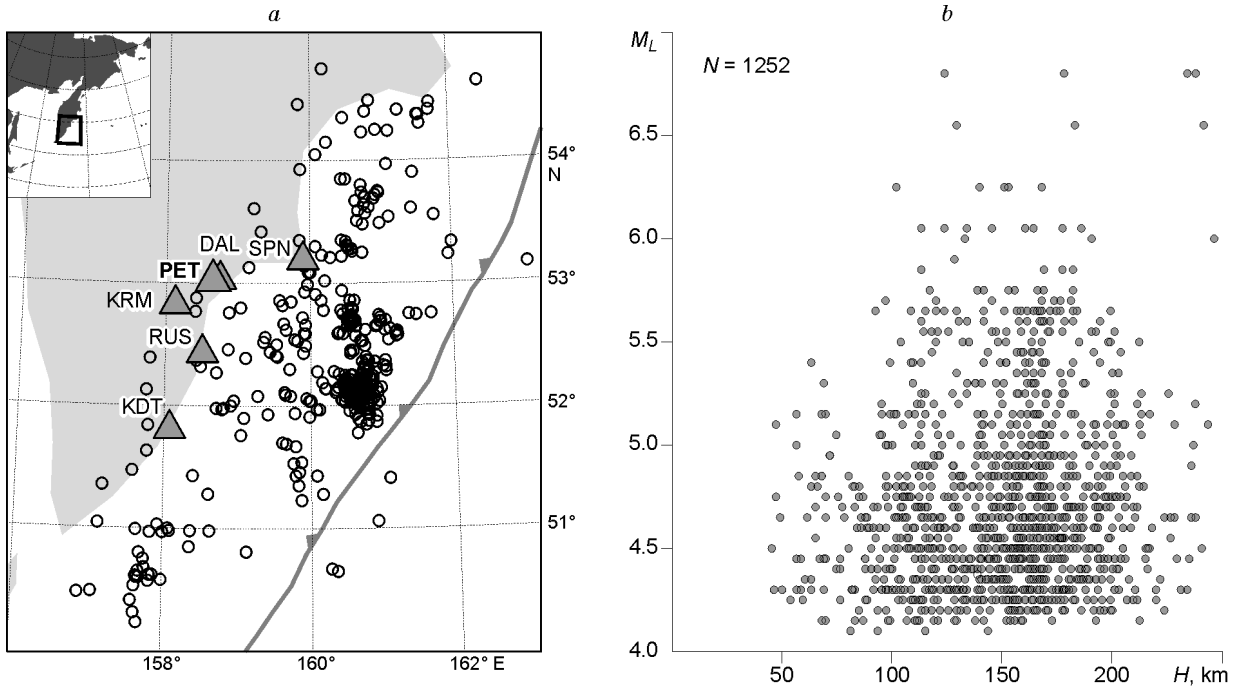

Fig. 1. *a,* Map showing the locations of the selected stations and earthquake epicenters; *b,* distribution of the recorded earthquake magnitudes and hypocentral distances. Here and below, *N* is the number of traces used (or calculated spectra).

frequency and makes a significant contribution to the effects of the real medium. In this study, the contribution of the factor $C_{21}(f)$ is taken into account using the quarter-wavelength approximation (Boore, 2003) based on the idea to use as $c_S^{(1)}\rho^{(1)}$ the average impedance in a subsurface layer of thickness $H(f)$, where $H(f)$ is determined from the condition

$$\frac{1}{4f} = \int_0^{H(f)} c_S^{-1}(l)\, dl, \qquad (2)$$

where dl is an element of the ray.

2.2. Frequency-dependent recording conditions near the receiver (local, near-surface geology, effect of relief, etc.) rarely reducible to a simple model of flat layers over half-space. This factor, $C_{22}(f)$, is also called the station spectral amplification. Under our conditions, it can only be estimated empirically, in relative units, setting $C_{22} = 1$ for a certain reference station with hard rock ground.

2.3. Inelastic loss in the medium. This factor distorts the signal shape only slightly, so that for a medium with homogeneous intrinsic loss and quality factor Q_i, it can be written as the spectral factor

$$C_{23}(f) = \frac{D_e(f)}{D(f)} = \exp\left(-\frac{\pi f r}{c_S Q_i(f)}\right) = \exp\left(-\frac{\pi f t}{Q_i(f)}\right), \qquad (3)$$

where $D(f)$ is the signal spectrum in a lossless medium and $D_e(f)$ is the same for a medium with loss.

3.1. Loss due to scattering (at large angles). Note that, according to the traditions of regional seismology (unlike, for example, optics), waves scattered at small angles are considered in combination with the direct wave (because their contributions are inseparable in practice), and this combination is interpreted as a direct wave. This approach has emerged in the absence of the expected single short pulse (or a series of pulses) in body-wave records, instead of which an extended noise-like signal is observed.

Thus, by analogy with (3), we introduce the scattering quality factor Q_{sc} and denote by $C_{31}(f)$ the analog of the factor $C_{23}(f)$ in which Q_i is replaced by Q_{sc}. Since the contributions of intrinsic loss and scattering to the loss are difficult to split, we will further use the total loss parameter $Q^{-1} = Q_i^{-1} + Q_{sc}^{-1}$ and the corresponding spectral coefficient for the direct wave

$$C_d(f) = C_{23}(f)\, C_{31}(f). \qquad (4)$$

3.2. The effects of multipath propagation and conversion at the boundaries. In the Kamchatka region, where S_n, S_g, L_g, etc., phases are almost unidentifiable, these effects are usually inseparable from the scattering effects. We will assume that the energy loss due to this factor is included in $C_d(f)$.

The total loss during propagation in homogeneous medium will be characterized by the parameter $\kappa = t/Q = r/cQ$. For the real medium, it is convenient to assume that κ has two components

$$\kappa = \kappa_0 + \kappa_v = \kappa_0 + \frac{r}{cQ(f, r)}, \qquad (5)$$

where $Q(f, r)$ characterizes the loss on the wave path propagation, except in a thin layer near the station, and κ_0 describes

Table 1. Accepted velocity profile for the PET station

H_{top}, km	0	0.025	0.25	0.5	1.5	4	29
c_P, km/s	1.4	2.6	2.6	4	5.5	6.3	6.3
c_S, km/s	0.8	1.4	1.7	2.0	2.8	3.6	3.6
ρ, kg/cm^3	2.1	2.1	2.2	2.4	2.7	2.8	3.3

the loss in this layer. Observations suggest that κ_0 (unlike κ_v) can be assumed to be independent of frequency.

Parameters and computational schemes for converting observed spectra to source spectra

To reduce the observed spectra to the ideal-case conditions, we needed to evaluate the contributions of the above factors according to Items 2.1, 2.2, 2.3, 3.1, and 3.2.

Calculation of impedance corrections. The reference station according to Item 2.2 was taken to be the PET station with high-impedance rock ground; the rationale for this choice is given in (Gusev and Guseva, 2016b; Pavlenko, 2013). To accomplish Item 2.1 for the conditions of the PET station, we used a profile (Table 1) compiled on the basis of (Gusev et al., 2009; Pavlenko, 2013). Calculation by (2) was made for a vertical ray. A graph of the function $C_{21}(f)$ is shown in Fig. 2.

Determination of station spectral corrections. The functions $C_{22}(f)$ (station spectral corrections) were determined for each station, e.g., SPN, as the average ratios of the *S*-wave and coda spectra for the same earthquake recorded at the SPN and PET stations. In the case of *S* waves, the spectra were previously reduced to a fixed $r = 1$ km taking into account the loss model (see below). In the case of coda waves, the ratio included station spectra of the coda segment of the same duration and with the same delay with respect to the origin time t_0. In both cases, the rms amplitude spectra of two horizontal components were used. The values of the ratios, denoted by H/H_{ref}, were averaged over earthquakes. In parallel, to compare the obtained ratios with independent data, we employed the popular Nakamura's technique (Nakamura, 1989) for estimating the spectral characteristics of the stations based on the ratio of spectra for the horizontal and vertical channels *(H/V)*. Figure 3 illustrates the calculation of the averaged ratios of *S*-wave and coda spectra for the RUS and NLC stations using 2011–2012 earthquake records. The averages over bands 0.5 Hz wide were calculated for the set of central frequencies of 0.5, 1.0, 1.5, ..., 25 Hz. For *S* waves, 117 spectra were used; for coda waves, 38 spectra; for some bands, the number of observations was somewhat smaller. Figure 4 shows the resulting ratios of the spectra for seven stations.

It is evident from Fig. 3 that the estimates from *S* waves and coda waves approximately agree with each other. However, the scatter of the coda-based estimates is much lower than that of the *S*-wave-based estimates ($\sigma(\log H/H_{ref})$ are of about 0.1 against 0.3). Nakamura's method demonstrates that, under our conditions, the *H/V* ratio has very limited capacity for estimating spectral anomalies, although the presence of anomaly is sometimes revealed more clearly. The *H/V* ratio was found to provide an accurate location of spectral peaks: at 4–6 Hz for NLC, and at about 2 Hz for KRM. However, the stable increase in the spectral corrections for RUS and KDT, which reaches a factor of 10 at 20–25 Hz for both *S* waves and coda waves, is not manifested in *H/V* ratios. The increase in the corrections with frequency, especially pronounced for RUS and KDT, presumably reflects the structure of the velocity profile beneath the stations in the upper tens of meters. Of interest is the presence, for RUS, of spectral corrections below unity at f less than 1.4 Hz, which has not been observed neither for the group of stations described here, nor for other stations and sites studied. We attribute this phenomenon to the geological setting of the RUS station. Beneath this station, there is a high-velocity block of granitoids, whereas beneath other stations, lower-velocity layers of shales and volcanites are located. Due to the strong resonance revealed near 5 Hz for the NLC station, we did not use its data to identify the corner frequencies of source spectra, because the smoothed correction function constructed by the method described above did not provide complete correction.

Thus, Nakamura's method could not reveal reliably station resonance effects, and as the final station corrections for the observed spectra we used the weighted mean corrections H/H_{ref} for two calculation methods, applying the weight of 2/3 to coda-based estimates and the weight of 1/3 to *S*-wave-based estimates.

Accounting for the attenuation during wave propagation. To calculate the factor $C_d(f)$, we used the results of (Gusev and Guseva, 2016a) for the loss parameters in the

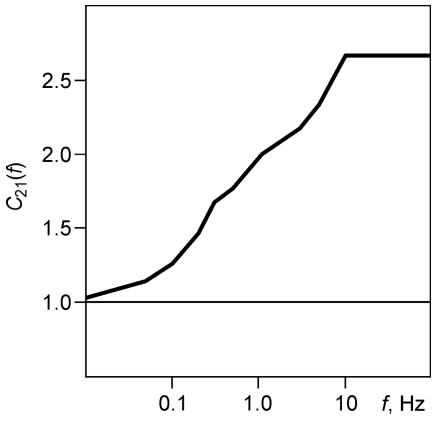

Fig. 2. Function $C_{21}(f)$ calculated using the quarter-wavelength approximation for the velocity profile presented in Table 1.

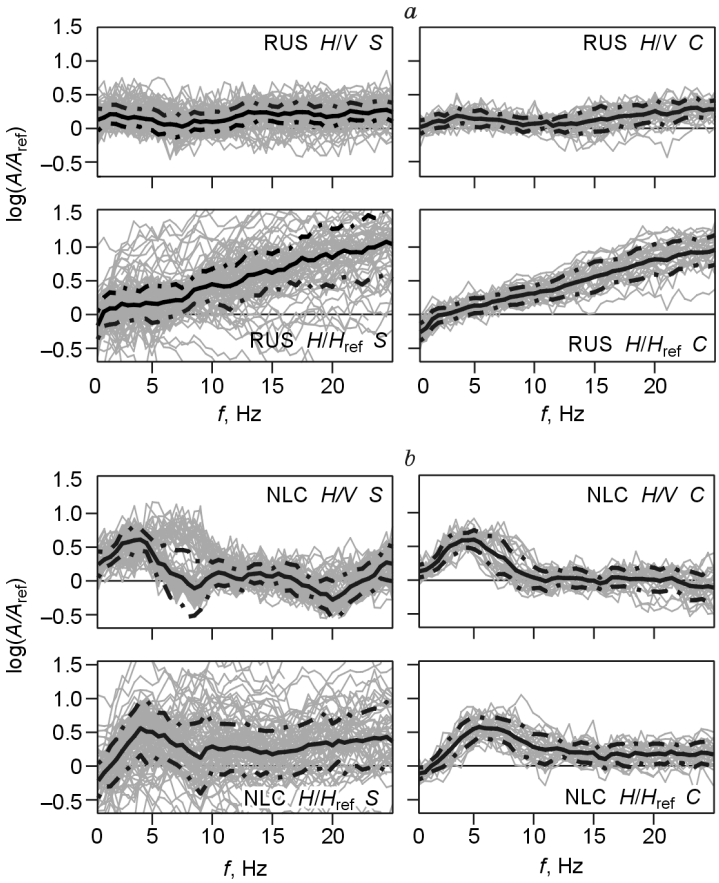

Fig. 3. Individual ratios of spectra A/A_{ref} for the RUS (*a*) and NLC (*b*) stations. In each case, four graphs are the individual (gray lines) and average (solid lines) ratios of spectra; the dot-dash line shows a robust estimate of the boundaries of the interval of ±1σ (based on interquartile range). The figure gives the ratios of the spectra of the horizontal and vertical components (*H/V*) and the ratios of the horizontal component of the station to the same for the PET station for *S* waves (*S*) and coda waves (*C*).

medium near the PET station. The Q function in (5) was assumed to have the form

$$Q^{-1}(f, r) = Q_0^{-1}\left(\frac{f}{f_0}\right)^{-\gamma}\left(1 + \frac{q(r - r_0)}{r_0}\right), \quad (6)$$

where f_0 = 1 Hz, r_0 = 100 km, Q_0 = 156, γ = 0.56, q = –0.08; and κ_0 = 0.03 s.

Thus, in the employed model for the formation of the signal spectrum, the coefficient A_1 in (1) is replaced by the spectral function $A_2(f) = C_t(f)\, A_1$, where

$$C_t(f) = C_{11}C_{12}C_{13}C_{21}(f)C_{22}(f)C_d(f). \quad (7)$$

In practical calculations, it was convenient to multiply the observed spectrum by the reduction coefficient $C_r(f) = r/C_t(f)$. As a result, we obtained the spectrum for the standard hypocentral distance r = 1 km. For these spectra, we will retain the notation $D(f)$, $V(f)$, and $A(f)$, and the original spectra will be redenoted as $D_0(f)$, $V_0(f)$, and $A_0(f)$.

Another important issue in the calculations is the selection of the time window of *S* waves for the calculation of their spectra. The start of the window was set 1.5 s before the time of arrival of *S* waves. In (Gusev and Guseva, 2016a), estimates of spectra were compared for two methods of selecting the end of the window: an interactive method, in which the selection was made visually at the end of the segment of large amplitudes of the *S* group, and an automatic method, where the window length was fixed as 25% of the travel time of *S* waves. The results differed only slightly. In this paper, we used the interactive method.

Estimation of source spectra and determination of corner frequencies

Calculation of smoothed spectra. Spectra were calculated using a specialized interactive program in Matlab (Fig. 5). It allows one to visualize original acceleration records, displacement traces calculated from accelerations, smoothed Fourier spectra of body waves in the versions $D(f)$, $V(f)$, and $A(f)$, control the quality of records and spectra, and determine corner frequencies. Corrections $C_r(f)$ are applied automatically. *S*-wave spectra obtained by FFT were reduced to r = 1 km and smoothed over bands 2/3 octave wide, and the density of the set of band central frequencies was taken as six points per octave.

Obtaining and controlling corner frequency estimates. Corner frequency estimates were obtained (if possible) interactively from the spectra. The sequence of the procedure is illustrated in Fig. 5. This procedure extends the method (Gusev

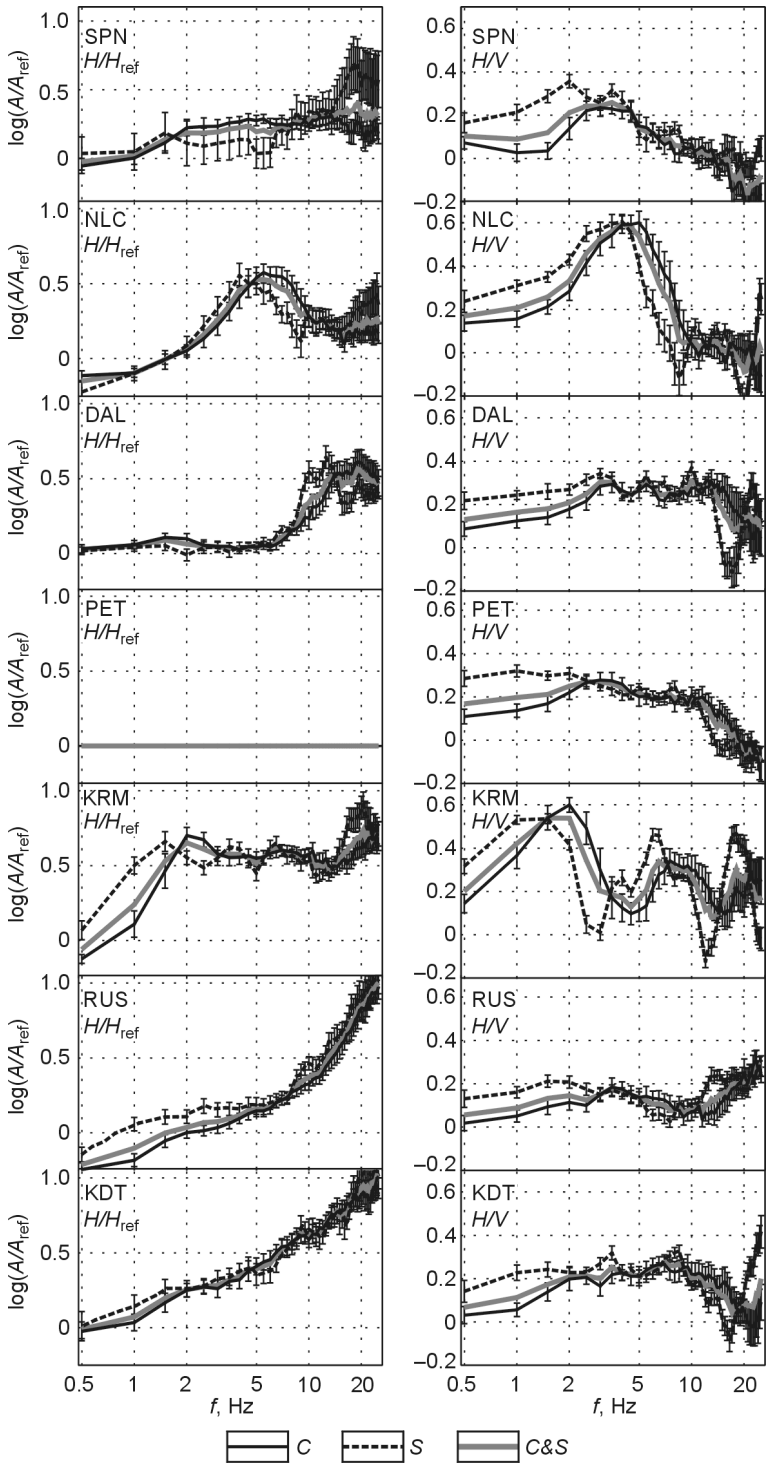

Fig. 4. Average ratios of the spectra of seven stations. The numerator of the ratios is the spectra for the horizontal channels. In the left column, the denominator of the ratios is the spectrum of the horizontal channel for PET; in the right column, the denominator is the spectrum of the vertical channel of the same station. *C,* calculation for coda waves; *S,* calculation for *S* waves; *C&S,* weighted mean of the two said estimates with weights of 2/3 and 1/3, respectively. The curve of *C&S* gives station corrections which were further used to reduce the observed spectra of other stations to the PET conditions. The vertical segments are the formal 95% confidence intervals for estimates of the average.

and Guseva, 2014). Totally, corner frequencies for 1252 spectra of *S* waves from 372 earthquakes were picked. We used only spectra that covered at least three octaves at a signal-to-noise (S/N) ratio of more than 2.5 (in amplitude). For f_{c3}, the spectrum sometimes could not be reduced to 20–25 Hz due to an unacceptable S/N ratio at higher frequencies or when the downward bend of the spectrum was not reliably detected. Estimates of f_{c3} were made only in the cases where the acceleration spectrum above the cutoff frequency decayed as f^{-1} or steeper within a band one-half octave wide

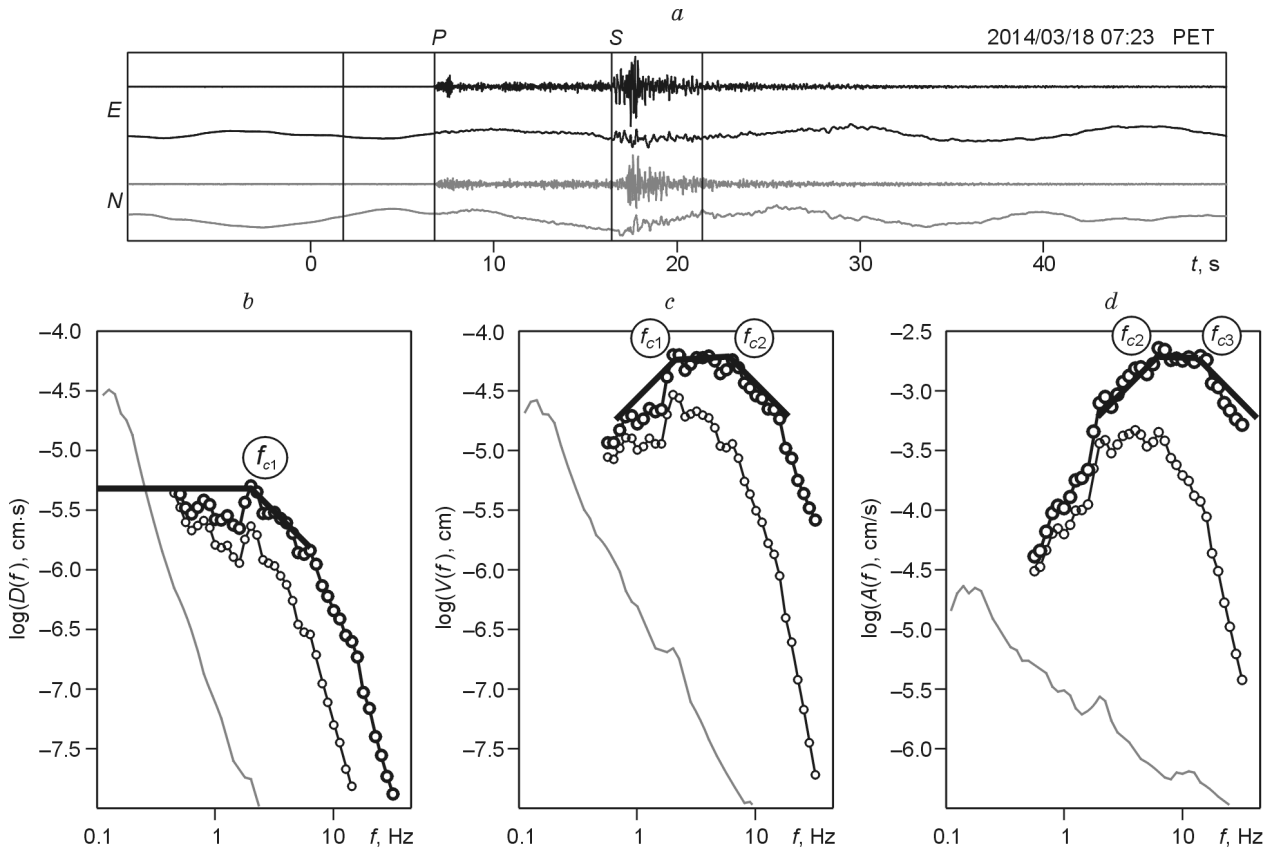

Fig. 5. Typical processing of *S* wave records, earthquake of 2014.03.18 at 07:23, $M_L = 4.2$, $r = 100$ km, $H = 46$ km. A copy of the dialog box is given. (*a*) From top to bottom: $A_0(t)$ and $D_0(t)$ for the *E* component, and below the same for the *N* component, PET station. The segments of the *S* group and noise are indicated by pairs of vertical lines. Below are graphs of the spectra of displacement (*b*), velocity (*c*), and acceleration (*d*). Curves in *b*, *c*, and *d*, from bottom to top: noise spectrum, $rD_0(f)$, and $D(f)$. Also shown is the interactively plotted polygonal line approximating $D(f)$; its breakpoints determine the choice of corner frequencies. *c, d,* similar curves for $V(f) = 2\pi f D(f)$ and $A(f) = (2\pi f)^2 D(f)$.

or wider. In cases of doubt, it was assumed that reliable information concerning f_{c3} could not be extracted, and such spectra were not used to estimate f_{c3}. We discarded 135 (11%) of the initial number (1252) of cases and retained 1117 cases of two kinds: with reliably observed f_{c3} (1028 cases or 92%, Fig. 6*a*) or with a flat spectrum up to 25 Hz (89 cases or 8%, Fig. 6*b*). From a content point of view, the last group includes cases where f_{c3} exists but is 25 Hz higher and therefore unobservable or cases where the true source displacement spectrum has an omega-square type asymptotics.

Also, there were often difficulties in estimating f_{c1}: instead of the expected distinct plateau of the spectrum $D(f)$ with reducing frequency, a growth in the spectrum was observed. The probable cause of this problem is the presence of an appreciable contribution of surface waves at low frequencies, which has also been observed in the same region previously (Abubakirov, 2005; Abubakirov and Gusev, 1990). Doubtful cases were excluded. The proportion of such cases is about 35%. It was always possible to pick the value of f_{c2}. It was not uncommon that $f_{c1} = f_{c2}$ or $f_{c2} = f_{c3}$.

Having picked the corner frequencies of source spectra, for each of the 1252 (source *i*)—(station *j*) pairs, we obtained a set (not always complete) of estimates of $\{f_{c1}, f_{c2}, f_{c3}\}$ with a total number of estimates of 839, 1252, and 1028, respectively: from 183 to 248 sets at each station.

Control of the internal consistency of corner frequency estimates

After obtaining the corner frequency estimates, we checked their internal consistency. In the first step, we compared the estimates of f_{c1}, obtained from graphs of the spectra of $D(f)$ and $V(f) = 2\pi f D(f)$ (Fig. 7*a*) and denoted by f_{c1}^D and f_{c1}^V. Similarly, estimates of f_{c2} were obtained from graphs of the spectra of $V(f)$ and $A(f) = 2\pi f V(f)$ (Fig. 7*b*) and denoted by f_{c2}^V and f_{c2}^A. In the ideal case, the estimates should coincide. The actual difference between the estimates of the two types is small (on average, less than 0.05 logarithmic units or 12%), which confirms the validity of the employed interactive technique of estimating corner frequencies. Next, the average values of $f_{c1} = (f_{c1}^D + f_{c1}^V)/2$ and $f_{c2} = (f_{c2}^V + f_{c2}^A)/2$ were used.

Another test was performed by comparing estimates for one event at several stations. Individual estimates of f_{ck} (k = 1, 2, 3) for each (source *i*)—(station *j*) combination will be

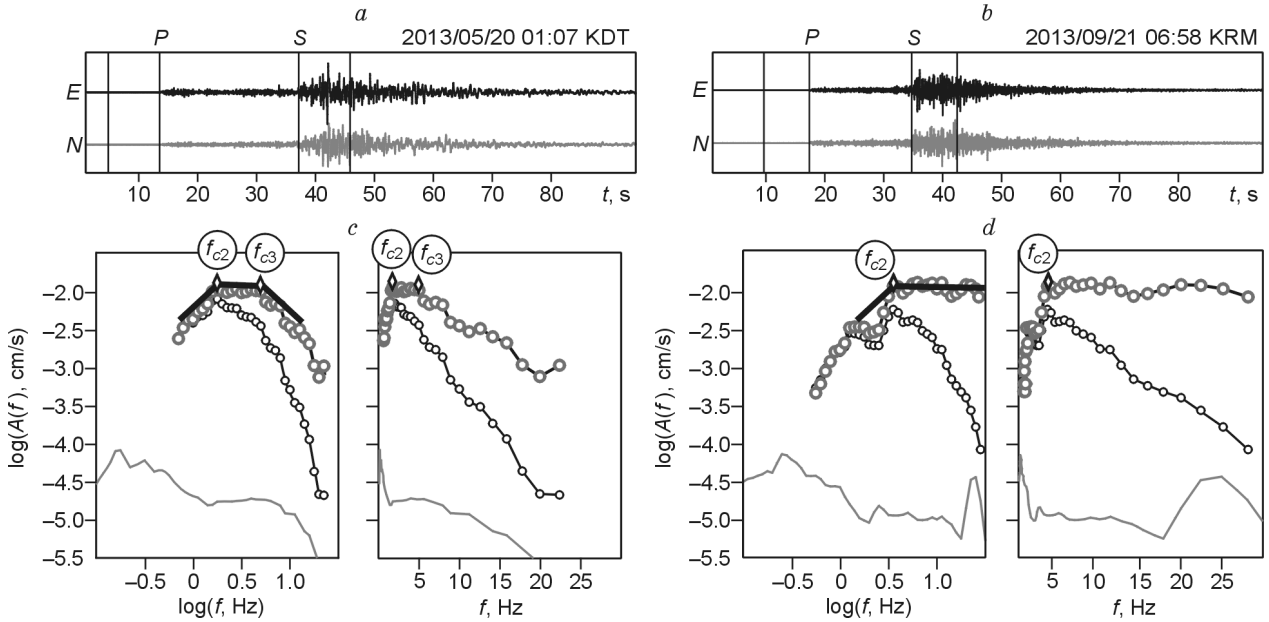

Fig. 6. Examples of acceleration spectra with distinct f_{c3} (*a*) and unobservable f_{c3} (*b*). Each block shows three graphs, of which the upper graph is an acceleration record and the lower two represent a smoothed acceleration spectrum. These two graphs display identical data but differ in the type of abscissa scale: it is logarithmic in the left graph and natural in the right graph. The notation is the same as in Fig. 5. Block (*a*) shows the record of the earthquake of 2013.05.20 at 01:07, $M_L = 5.8$, $r = 160$ km, $H = 55$ km at the KDT. Block (*b*) shows the record of the earthquake of 2013.09.21 at 06:58, $M_L = 5.6$, $r = 149$ km, $H = 46$ km at the KRM. Noteworthy is the complete invisibility of f_{c3} in the left graph in the natural scale, especially in the uncorrected spectrum. Such cases are common; in the standard approach to estimating κ, there may be biased estimate of loss.

denoted by $f_{ck}^{(ij)}$, where $j = 1, 2, ..., n$, $n \le 6$; mainly $n \ge 4$. The network-averaged (over all j) value of $\log f_{ck}^{(ij)}$ will be denoted by $\log f_{ck}^{(i)}$. The residuals $\delta_k^{(ij)} = \log f_{ck}^{(ij)} - \log f_{ck}^{(i)}$ were calculated. Figure 8 shows histograms of the residuals $\delta_k^{(ij)}$ for $k = 1$, 2, and 3. It is seen that the corresponding distributions are close to the normal law. For each i, the variance of $\log f_{ck}^{(ij)}$ was estimated as

$$\sigma_k^{2(i)} = \frac{1}{n-1} \sum_{j=1,\ldots,n} \delta_k^{2(ij)} \qquad (8)$$

and the results were averaged over all i to obtain the average variance σ_k^2. The values of σ_k for the residuals $\delta_k^{(ij)}$ of the estimates of $\log f_{c1}$, $\log f_{c2}$, and $\log f_{c3}$ are 0.17, 0.14, and 0.11, respectively; this is the accuracy of single estimates. The relative accuracy of the estimates of f_{ck} averaged over n stations can be obtained as $\varepsilon_k = \sigma(\ln f_{ck})/n^{0.5} = 2.3\sigma_k/n^{0.5}$, which, for typical $n = 4$, is 20 to 13%. The obtained accuracy estimates are deemed acceptable.

Scaling properties of corner frequencies

After making sure that the obtained estimates are internally consistent, we further studied the scaling pattern for f_{c1}, f_{c2}, and f_{c3}, i.e., we checked the existence of dependences $f_{ck} \sim M_0^{-\beta_k}$ and found estimates of the exponent β_k. The seismic moment was obtained from the moment magnitude estimated from the regional Kamchatka magnitude M_L using the simplified temporary formula

$$M_{W(L)} = M_L - 0.20. \qquad (9)$$

To test the validity of this formula, we compared M_L of the studied earthquakes and the value of M_W calculated from M_0 determined by the GCMT survey. The data are approximately consistent with a relationship pattern in the form of a constant relative shift.

Dependences of the estimates of f_{c1}, f_{c2}, and f_{c3} on $M_{W(L)}$ are presented in Fig. 9. The scaling properties for f_{c1} have been well studied in the literature. For $M > 6$, it is usually close to $f_{c1} \sim M_0^{-1/3}$, and this dependence indicates kinematic and dynamic similarity between the source processes at different magnitudes. The issue of the scaling pattern for $M < 6$ is controversial. Some authors believe that here, too, similarity holds, while others have found that β_1 is substantially below 1/3. Ordinary linear regression was carried out assuming a linear relationship between $\log f_{c1}$ and $M_{W(L)}$. We also used orthogonal regression in view of the probable existence of inaccuracies in the estimates of M_L. In this case, the ratio of the standard deviations for $\log f_{ck}$, with respect to M_L, was set equal to two (with some margin). Orthogonal regression results were considered preferable. Similar processing was conducted for f_{c2} and f_{c3}. Linear relationships are indeed observed (Fig. 9*a–c*, Table 2). Estimates of the slope of b_k are converted to estimates $\beta_k = -d\log f_{ck}/d\log M_0$ by multiplying by 2/3.

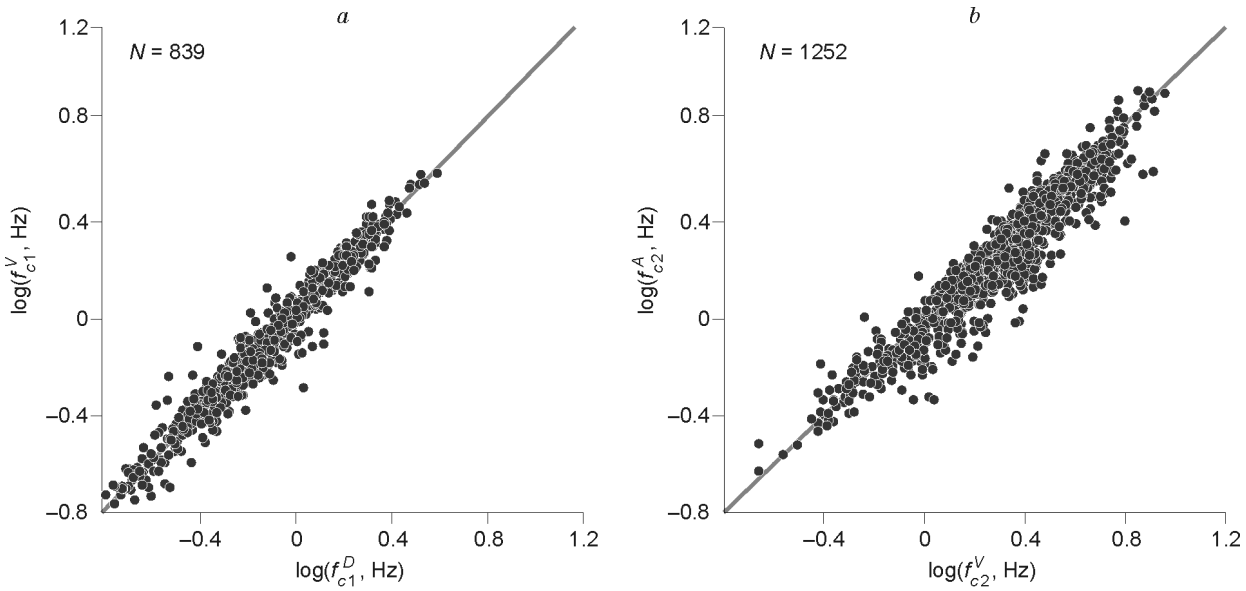

Fig. 7. Check of the agreement between estimates of f_{c1} and f_{c2} taken in different dialog boxes. *a*, f_{c1}^{D} in comparison with f_{c1}^{V}; *b*, f_{c2}^{V} in comparison with f_{c2}^{A}. The average difference $f_{c1}^{V} - f_{c1}^{D}$ and the corresponding standard deviation are 0.04 and 0.06 (*a*); the same parameters for $f_{c2}^{A} - f_{c2}^{V}$ are 0.07 and 0.09 (*b*).

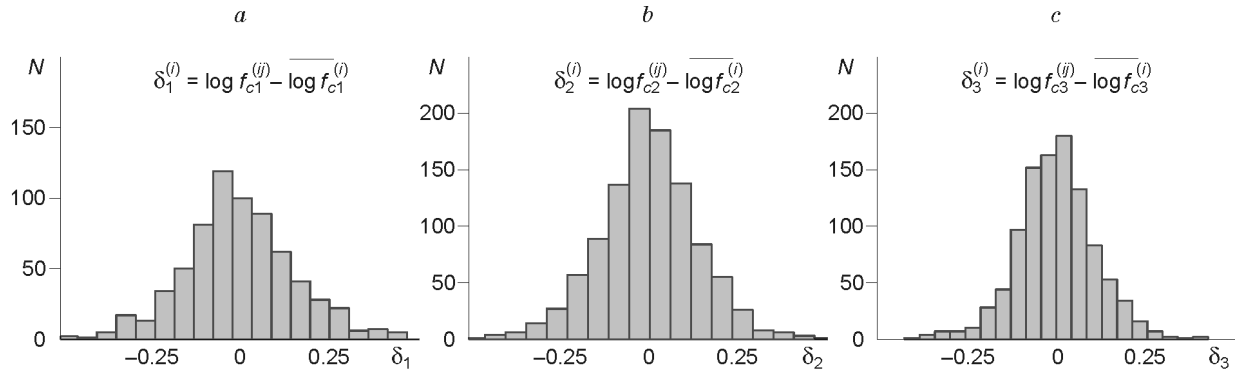

Fig. 8. Histograms of residuals $\delta_k^{(ij)}$ (station minus network-averaged) for the estimates of the first f_{c1} (*a*), second f_{c2} (*b*), and third f_{c3} (*c*) corner frequencies.

It is evident from Table 2 that the slope of the relationship $\log f_{c1}(M_{W(L)})$, $b_1 = 0.42$ obtained by ordinary regression is different from the value of 0.5 expected in the case of similarity. Although this difference is formally significant, it is unlikely to be realistic: in view of the presumed inaccuracy of the values of M_L, the value of b_1 can reach 0.51. However, an accurate estimate is difficult to obtain as the true ratio of the accuracies is not known exactly. It can be assumed that the true b_1 is in the range 0.42–0.51, so that β_1= 0.28–0.34. This is an important result: the indicated interval includes the value β_1 = 1/3 expected within the framework of the similarity hypothesis, so that the data are rather consistent with this hypothesis. In any case, this result is preliminary since the large proportion of discarded data f_{c1} might lead to wrong conclusions.

Unlike f_{c1}, the behavior of f_{c2} and f_{c3} is poorly known and is of great interest. Furthermore, in these cases, the loss of data was not as prominent as in the case with f_{c1}. Therefore it can be assumed that the obtained trends are largely realistic: $\beta_2 = 0.23 \pm 0.01$ and $\beta_3 = 0.13 \pm 0.01$. The values of β_2 and especially β_3 are significantly below 1/3, indicating a violation of the assumption of similarity. This is an important result of the work.

Discussion

This study extends the previous research (Gusev and Guseva, 2014). The significant advance is due to the fact that, instead of a single station, we used a network of stations with a refined loss model (Gusev and Guseva, 2016a) and impedance corrections; in addition, a new set of seismograms is used in this paper.

Mention should be made of the not infrequent cases where the plateau in the spectrum $A(f)$ was not exactly horizontal (as in Fig. 5*d*). It is clear that this effect is due to the use of a single attenuation model for all source-receiver traces, which

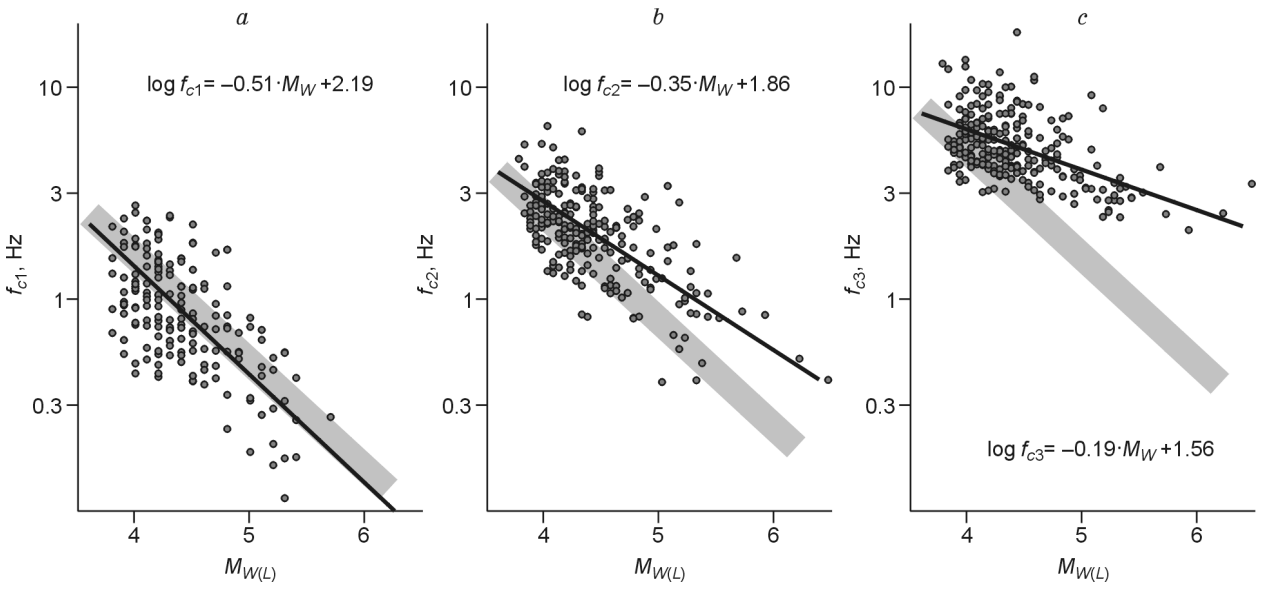

Fig. 9. Corner frequencies f_{c1}, f_{c2}, and f_{c3} determined from *S* wave spectra versus magnitude $M_{W(L)}$ (black line) obtained by orthogonal regression. Straight lines with a slope of –0.5 (gray lines) corresponding to the relation $f_{ck} \propto M_0^{-1/3}$ are drawn (at an arbitrary level) for comparison. It can be seen that these f_{c1} roughly follow the trend expected according to the similarity hypothesis, while the trends for f_{c2}, and especially for f_{c3} contradict this hypothesis.

is an idealization. The main thing that allows us to be sure that the key results of the study are reliable, i.e., that the third corner is indeed present in the spectrum and the estimates of f_{c3} are realistic, is the absence of a systematic underestimation of the loss. Otherwise, instead of the approximately horizontal plateaus, we would have obtained systematically inclined (to the right) plateaus in the spectra $A(f)$. This trend was not observed: we obtained limited slopes of both signs. This suggests that most of the estimates of f_{c3} obtained in the study are not significantly biased.

Estimates of β_2 and β_3 for other regions are listed in (Aki, 1988), where it is also noted that the value of β_2 is generally close to 0.17, which is comparable to our estimate of 0.23. For β_3, published estimates are less reliable, but the early estimate $\beta_3 = 0.12$ from (Faccioli, 1986) is confirmed in the present study (0.13). Estimates from (Gusev and Guseva, 2014) are also comparable. Thus, the identified scaling parameters for f_{c2} and f_{c3} are in agreement with earlier studies.

Below, we briefly summarize the hypotheses (Gusev and Guseva, 2016a,b) on the possible nature of the detected scaling trends. The value of f_{c2} correlates with the width of the rupture front forming the source area, while the value of f_{c1} correlates with the size of this area. The ratio of the estimates β_2/β_1 is about 0.5, which may indicate that, with increasing source size, the front width increases according to the well-known "random walk with drift" stochastic mechanism.

The value of f_{c3} correlates with the upper cutoff of the wavenumber spectrum of the strength and (or) stress drop field at the fault. This cutoff can be formed due to the wear of the surface of the fault walls. The wear leads to abrasion of small protrusions and disappearance of the fine details of the profile, which suppresses high-frequency radiation. The slow increase in f_{c3} with M_0 may indicate that larger earthquakes often originate at more mature and more worn-out faults.

From a practical point of view, the results are useful to clarify the meaning of empirical estimates of the parameters κ and (or) κ_0. Although the estimation of these attenuation parameters from spectra of accelerograms has become a standard practice in modern earthquake engineering, the possibility of the partial source origin of this parameter is usually completely ignored. Accounting for the source contribution to the distance decay of the observed acceleration spectrum can help not only to improve estimates for κ_0, but also to correct the possible bias of estimates of κ (i.e., of Q).

Table 2. Regression analysis of scaling relationships $\log f_{ck} = a_k - b_k M_{W(L)}$ using linear regression versions

Parameter	N	Orthogonal regression*						Ordinary regression					
		a_k	sa_k	b_k	sb_k	s_k	R	a_k	sa_k	b_k	sb_k	s_k	R
$\log f_{c1}$	173	2.19	0.18	0.51	0.04	0.21	0.62	1.71	0.17	0.40	0.04	0.21	0.62
$\log f_{c2}$	234	1.86	0.10	0.35	0.02	0.16	0.67	1.69	0.10	0.31	0.02	0.16	0.67
$\log f_{c3}$	235	1.56	0.09	0.19	0.02	0.14	0.50	1.48	0.09	0.17	0.02	0.14	0.50

Note. sa_k and sb_k are the standard deviations for estimates of a_k and b_k; s_k is the rms residual; R is the determination coefficient; $k = 1, 2, 3$.
* Preferred version.

Conclusions

A considerable number of estimates of three corner frequencies of source spectra for Eastern Kamchatka earthquakes was obtained using a significantly modified approach to data analysis. This approach allowed considerable progress in demonstrating the existence of the poorly known parameter of source-controlled f_{max}, which was denoted by f_{c3}—the third corner frequency. The other two corner frequencies f_{c1} and f_{c2} were also studied.

The results of this study support a number of previously published findings obtained in the same region based on the data of a single station and a different set of records. Again, common presence of the third corner in source spectra has been revealed; again, it has been found that the common law of similarity of source spectra ($\log f_c = 1/3 \log M_0 + \text{const}$) does not hold for f_{c2} nor f_{c3} but is relatively acceptable for f_{c1}.

The results significantly complement our understanding of the properties of the earthquake sources in the seismically active Kamchatka region. The observed common presence of the upper cutoff of source spectra is important for problems of engineering seismology. The existence of f_{c3} should be taken into account in estimating the station parameter κ_0 and the amplitude decay with distance. On the other hand, an accurate prediction of the parameters of possible strong motions should consider f_{c3} as one of the parameters determining the source spectrum of devastating earthquakes and thus their effect on the site.

The study was supported by a grant from the Russian Science Foundation No. 14-17-00621 to the Kamchatka Branch of the Geophysical Survey, Russian Academy of Sciences.

References

Abubakirov, I.R., 2005. Attenuation characteristics of transverse waves in the lithosphere of Kamchatka estimated from observations at the Petropavlovsk digital broadband station. Izv. Phys. Solid Earth 41 (10), 813–824.

Abubakirov, I., Gusev, A., 1990. Estimation of scattering properties of lithosphere of Kamchatka based on Monte-Carlo simulation of record envelope of a near earthquake. Phys. Earth Planet. Inter. 64, 52–67.

Aki, K., 1967. Scaling law of seismic spectrum. J. Geophys. Res. 7, 1217–1231.

Aki, K., 1988. Physical Theory of Earthquakes. Seismic Hazard in Mediterranean Region. Kluwer Academic Publishers, pp. 3–33.

Anderson, J., Hough, S., 1984. A model for the shape of the Fourier amplitude spectrum of acceleration at high frequencies. Bull. Seismol. Soc. Am. 74, 1969–1993.

Boore, D., 2003. Simulation of ground motion using the stochastic method. Pure Appl. Geophys. 160, 635–676.

Brune, J., 1970. Tectonic stress and the spectra of seismic shear waves from earthquakes. J. Geophys. Res. 75, 4997–5009.

Chebrov, V.N., Droznin, D.V. Kugaenko, Yu.A., Levina, V.I., Senyukov, S.L., Sergeev, V.A., Shevchenko, Y.V., Yashchuk, V.V., 2013. The system of detailed seismological observations in Kamchatka in 2011. J. Volcanol. Seismol. 7 (1), 16–36.

Faccioli, E., 1986. A study of strong motions from Italy and Yugoslavia in terms of gross source properties. Geophys., Monograph 37, Maurice Ewing Series 6, 297–309.

Gusev, A., 1983. Descriptive statistical model of earthquake source radiation to an estimation of short-period strong motion. Geophys. J. R. Astron. Soc. 74, 787–808.

Gusev, A., 2012. High-frequency radiation from an earthquake fault: a review and a hypothesis of fractal rupture front geometry. Pure Appl. Geophys. 170 (1–2), 65–93.

Gusev, A.A., Guseva, E.M., 2014. Scaling properties of corner frequencies of Kamchatka earthquakes. Dokl. Akad. Nauk 458, No. 1, 88–91.

Gusev, A.A., Guseva, E.M., 2016a. Shear wave attenuation estimated from the spectral decay rate in the vicinity of the Petropavlovsk station, Kamchatka. Izv. Phys. Solid Earth 52 (4), 503–519.

Gusev, A.A., Guseva, E.M., 2016b. Source spectra of near Kamchatka earthquakes: recovering them from *S*-wave spectra, and determination of scaling for three corner frequencies. Pure Appl. Geophys. 173, 1539–1557.

Gusev, A.A., Guseva, E.M., Pavlov, V.M., 2009. Modeling of the ground motion for the Petropavlovsk earthquake of November 24, 1971 ($M = 7.6$). Izv. Phys. Solid Earth 45 (5), 395–405.

Hanks, T., 1982. f_{max}. Bull. Seismol. Soc. Am. 72, 1867–1879.

Nakamura, Y., 1989. A method for dynamic characteristics estimations of subsurface using microtremors of ground surface. QR RTI 30, 25–33.

Papageorgiou, A., Aki, K., 1983. A specific barrier model for the quantitative description of inhomogeneous faulting and the prediction of strong ground motion. 1. Description of the model. Bull. Seismol. Soc. Am. 73, 693–722.

Pavlenko, O., 2013. Simulation of ground motion from strong earthquakes of Kamchatka region (1992–1993) at rock and soil sites. Pure Appl. Geophys. 170 (4), 571–595.

Purvance, M., Anderson, J., 2003. A comprehensive study of the observed spectral decay in strong-motion accelerations recorded in Guerrero, Mexico. Bull. Seismol. Soc. Am. 93, 600–611.

Editorial responsibility: V.S. Seleznev